

**Joshua D. Davis**<sup>1</sup>

Robot and Protein Kinematics Lab,  
Department of Mechanical Engineering,  
Johns Hopkins University,  
Baltimore, MD 21218  
e-mail: jdavi160@jhu.edu

**Michael D. Kutzer**

Weapons and Systems Engineering,  
United States Naval Academy,  
Annapolis, MD 21401  
e-mail: kutzer@usna.edu

**Gregory S. Chirikjian**

Robot and Protein Kinematics Lab,  
Department of Mechanical Engineering,  
Johns Hopkins University,  
Baltimore, MD 21218  
e-mail: gregc@jhu.edu

# Algorithms for Multilayer Conformal Additive Manufacturing

*Despite the rapid advance of additive manufacturing (AM) technologies in recent years, methods to fully encase objects with multilayer, thick features are still undeveloped. This issue can be overcome by printing layers conformally about an object's natural boundary, as opposed to current methods that utilize planar layering. With this mindset, two methods are derived to generate layers between the boundaries of initial and desired geometric objects in both two and three dimensions. The first method is based on variable offset curves (VOCs) and is applicable to pairs of initial and desired geometric objects that satisfy mild compatibility conditions. In this method, layers are generated by uniformly partitioning each of the normal line segments emanating from the initial object boundary and intersecting the desired object. The second method is based on manipulated solutions to Laplace's equation and is applicable to all geometric objects. Using each method, we present examples of layer generation for several objects of varying convexities. Results are compared, and the respective advantages and limitations of each method are discussed. [DOI: 10.1115/1.4033047]*

## 1 Introduction

The exponential growth of AM or 3D printing technologies in recent years has led to rapid adoption by both the public and private sectors. In 2013, the Chief Naval Officer's Rapid Innovation Cell began the Print the Fleet (PTF) project aimed at leveraging AM technology on Naval vessels. The underlying motivation for the project is to ultimately enable rapid adaptation in the "changing landscape of warfare" [1]. Recent PTF initiatives include the evaluation of AM technology on an unarmed joint high speed vessel and the sponsoring of a permanent installation of AM technology onto the USS Essex [1,2]. In a parallel effort, NASA evaluated AM technology in zero-gravity environments with a demonstration system recently deployed on the International Space Station [3]. The goal of this experiment was to demonstrate that a 3D printer works normally in a zero-gravity environment. The ultimate goal for projects like these is to enable rapid, on-site repair, replacement, and adaptation of mechanical (and potentially electrical) hardware.

Commercial AM technology leverages a variety of processes to bind materials, creating solid structures. Unlike traditional fabrication methods, a direct correlation between AM fabrication-time and part complexity does not necessarily exist. AM fabrication also offers relaxed design rules and simple part-by-part customization. As a result, inexperienced developers can produce physical hardware almost immediately, while experienced designers can create complex parts tailored for specific applications. Table 1 summarizes current commercial AM technologies by process [4].

As adoption of AM increases, the limitations of current technology will become more distinct. Recent research in AM processes is focused on addressing limitations in properties of printed materials [5–8]; however, existing methods have yet to be exploited to

their full potential. While current AM enables tremendous innovation in part design, designers are still required to follow classical packaging and/or assembly rules. Examples include retrofits (e.g., USS Whidbey Island prototype adapter brackets [1]), packaging (e.g., electronics and sensors), and repair.

In current AM, parts are made by iteratively adding layers of material. Layers are defined by thin cross sections of a part, and derived from an exported computer-aided design (CAD) model [9]. Commercial AM techniques generally use a "build-bed" that serves as the flat substrate for part fabrication. The CAD model is imported into an AM software package, and positioned relative to the build-bed. Layers are then defined by equally spaced planar slices of the CAD model, parallel to the build-bed. This is effective for a wide variety of part geometries. Depending on the AM process, issues may arise with overhanging features, but this limitation is effectively solved by adding sacrificial support layers that are removed following the completion of the AM process [9]. Because of this, no AM technology is currently capable of manufacturing a closed, fully hollow feature. A graphical example of the differences between "traditional" planar printing and conformal printing is provided in Fig. 1.

The concept of conformal printing onto nonplanar surfaces has been explored for a variety of applications including subtractive processes like lithography used to produce optics [10,11], and additive methods to fabricate antennas and electronics onto/into mechanical components [12–14]. In general, the AM techniques explored for conformal applications involve "direct write" technologies [9] used to produce thin features on surfaces. More specifically, most current techniques have only demonstrated the deposition of a single layer of material [12,14]. On the other hand, additional material extrusion methods such as curved layer fused deposition introduced in Refs. [15] and [16] can generate nonplanar surfaces at the cost of requiring a large amount of sacrificial support material.

Leveraging new layering concepts in conjunction with registration and manipulation methods commonly used in robotics, conformal AM can be extended to incorporate multilayer, thick features. Additionally, conformal AM can be used to produce seamless packaging, repair damaged hardware, incorporate heterogeneous materials into products to provide extra strength and/or

<sup>1</sup>Corresponding author.

Contributed by the Design Engineering Division of ASME for publication in the JOURNAL OF COMPUTING AND INFORMATION SCIENCE IN ENGINEERING. Manuscript received December 24, 2015; final manuscript received February 28, 2016; published online April 15, 2016. Editor: Bahram Ravani.

This material is declared a work of the U.S. Government and is not subject to copyright protection in the United States. Approved for public release; distribution is unlimited.

**Table 1 Summary of commercial AM technologies**

Process	Description	Material(s)	Manufacturer(s)
Binder jetting	A liquid bonding agent is selectively deposited to join powder materials	Polymers, sand, glass, metals	3D Systems, ExOne
Direct energy deposition	Focused thermal energy is used to fuse materials by melting as they are deposited	Metals	Optomec, POM
Material extrusion	Material is selectively dispensed through a nozzle or orifice	Polymers	Stratasys, Bits from Bytes, MakerBot, RepRap
Material jetting	Droplets of build material are selectively deposited	Polymers, waxes	Objet, 3D Systems
Powder bed fusion	Regions of material are selectively fused in a powder bed using sintering or melting	Metals, polymers	3D Systems, EOS, Arcam
Sheet lamination	Sheets of material are bonded to form an object	Paper, metals	Fabrisonic, Mcor, Cubic Technologies
Vat photopolymerization	Liquid photopolymer in a vat is selectively cured by light-activated polymer	Photopolymers	3D Systems, Envisiontec, OS-RC, Formlabs, Kudo3D

durability, and provide retrofitting capabilities (for example, adding a handle or flange to an existing piece of hardware).

This paper presents new approaches to conformal AM. Two methods are presented to construct multiple enveloping layers around an initial object that result in a desired final object. Each method assumes two inputs (the boundary of the initial object, and the boundary of the desired object) described in a common reference. The first method utilizes VOCs to generate layers, and is limited to pairs of initial and final desired geometric objects that satisfy certain mild compatibility conditions. The second method leverages solutions to Laplace’s equation, and is applicable to all pairs of geometric objects with differentiable boundaries. Next, we develop a process that alters the layers generated by these methods to incorporate 2D and 3D hollow features (or voids). For completeness, several 2D and 3D applications of each method (with and without voids) are presented. Results demonstrate successful layering for each method, and advantages and limitations of the presented methods are discussed. This layering approach, depending on the physical implementation, is applicable to a wide range of AM processes. However, in the near-term, this method is most readily applied to material extrusion methods such as fused deposition modeling or FDM.

**2 Desired Properties for Conformally Printed Layers**

In contrast to a majority of current AM methods that deposit material in a fixed plane, conformal AM methods deposit layers along closed curves for 2D objects and along surfaces for 3D objects. This distinction lends itself to a new definition of layers in conformal AM processes.

As a result, we define each layer as a bijective mapping between an initial curve/surface and each layer (including the desired curve/surface). Intuitively, this mapping ensures that each point on the initial boundary maps uniquely to a point on each layer, and that each layer is a closed curve/surface. This mapping guarantees that layers will not intersect and are thereby unique. Physically, this mapping ensures that material will never be deposited at the same point twice. Additionally, this method prevents arbitrary areas without material deposition (unless specified) between subsequent layers provided proper layer thickness and continuity [17].

**3 Layer Generation Using VOCs**

Given a parametrized curve  $\mathbf{x}_0(t)$ , a VOC is defined as

$$\mathbf{x}_1(t; r) = \mathbf{x}_0(t) + r(t)n(t) \tag{1}$$

where  $r(t) \in \mathbb{R}^+$  is a parametrically varying scalar and  $n(t)$  is the unit normal to the curve. Offset curves, and their more general counterparts VOCs, are well-established in the literature with several papers providing in-depth analysis of their analytical and algebraic properties [18–21]. Note that by an abuse of terminology, variable offset surfaces will also be included in our definition of VOCs. In addition, for the remainder of this section we will assume that every curve or surface is closed and at least  $C^2$  continuous. Finally, further restrictions must be imposed to ensure that there is a bijective mapping between our initial boundary (curve/surface) and each layer.

ASSUMPTION 1. *The boundary of the initial object is convex and fully contained inside of the boundary of the desired object.*

In this context, a boundary  $S$  is convex if for all points  $z_1$  and  $z_2$  in  $S$  and  $\alpha \in [0, 1]$ , it follows that

$$\alpha z_1 + (1 - \alpha)z_2 \in S_i \tag{2}$$

where  $S_i$  is the union of the boundary with its interior.

ASSUMPTION 2. *The boundary of the desired object is of a “compatible” nature with respect to the boundary of the initial object, meaning that each point on the boundary of the desired*

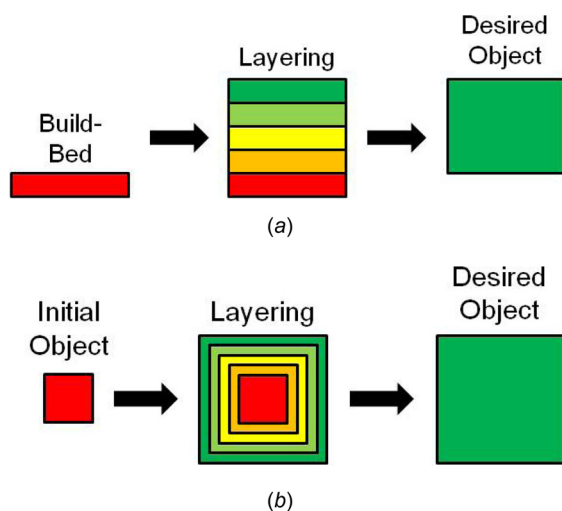


**Fig. 1 Comparison of cross-sectional views for a printed object**

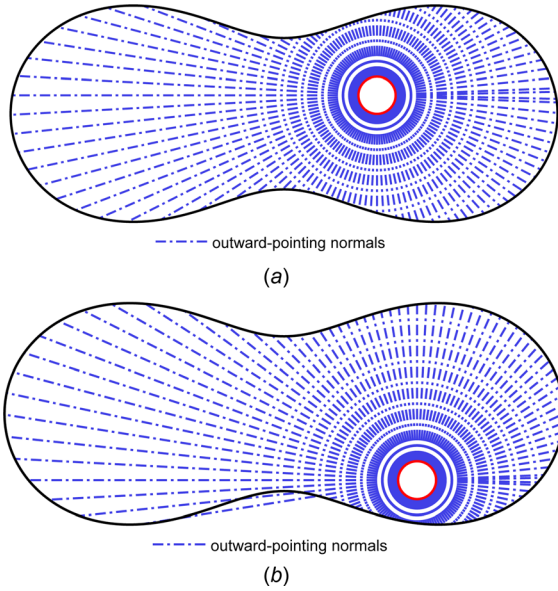


**Fig. 2** An example of the dependence of a compatible desired object on the position of the initial object (a) a compatible desired object and (b) a incompatible desired object

object intersects exactly one outward-pointing normal ray emanating from the initial object's boundary.

This definition ensures that the VOC method will fully reconstruct the boundary of the desired object for any given convex initial object (i.e., there will be no gaps on the boundary of the desired object that remove curvature, changes in convexity, or other features). Additionally, one may infer from the definition above that the compatibility of a desired object is highly dependent on the position and orientation of the initial object. Figure 2 highlights this linkage by providing two examples with the same initial and desired objects; in the first example (Fig. 2(a)) the desired object is compatible and in the second (Fig. 2(b)) it is not due to some outward-pointing normals intersecting the boundary of the desired object multiple times.

Our first assumption prevents outward-pointing normal vectors of the boundary of the initial object from intersecting one another, while our second assumption ensures that every outward-pointing normal will intersect the boundary of the desired object at exactly one point. Moreover, each point of intersection is unique and the set of all points of intersection recover the boundary of the desired object.

**3.1 Two-Dimensional Formulation.** For the planar case, we desire two  $C^2$  functions representing the initial and desired curves; however, in many practical applications, curves are approximated by a discrete number of points. Therefore, given two ordered sets of points,  $\mathbf{U} = \{\mathbf{u}_1, \mathbf{u}_2, \dots, \mathbf{u}_n\}$  and  $\mathbf{V} = \{\mathbf{v}_1, \mathbf{v}_2, \dots, \mathbf{v}_m\}$ , we use piecewise parametric cubic splines to generate the initial and desired closed curves  $\gamma_0$  and  $\gamma_1$ , with  $\gamma_0 \subsetneq \gamma_1$ . Each parametric spline is described as a cubic polynomial of the form

$$\mathbf{X} = \mathbf{a}t_0^3 + \mathbf{b}t_0^2 + \mathbf{c}t_0 + \mathbf{d} \quad (3)$$

where  $\mathbf{X} = [x, y]^T \in \mathbb{R}^2$ ,  $\mathbf{a}, \mathbf{b}, \mathbf{c}$ , and  $\mathbf{d}$  are coefficients that uniquely describe the spline, and  $t_0 \in [0, 1)$  represents the interval on which the spline is valid. For the remainder of this section, we will append superscripts to the spline coefficients (e.g.,  $\mathbf{a}^0$ ) to distinguish between the splines representing  $\gamma_0$  and  $\gamma_1$ .

Tangent vectors for  $\gamma_0$  are calculated by taking the derivative of the cubic splines with respect to the parametric variable  $t_0$ .

$$\mathbf{T} = \frac{d\mathbf{X}}{dt_0} = 3\mathbf{a}^0t_0^2 + 2\mathbf{b}^0t_0 + \mathbf{c}^0 \quad (4)$$

Normal vectors are derived by appending a zero to the tangent vector and taking the cross product with the appropriate unit vector that completes a right-handed frame

$$\mathbf{N} = \begin{bmatrix} T_1 \\ T_2 \\ 0 \end{bmatrix} \times \begin{bmatrix} 0 \\ 0 \\ 1 \end{bmatrix} = \begin{bmatrix} T_2 \\ -T_1 \\ 0 \end{bmatrix} \quad (5)$$

Remembering, from Assumption 1, that outward-pointing normal vectors projected from the boundary of convex objects do not intersect one another, we construct parametric lines beginning on the boundary of  $\gamma_0$  and extending to  $\gamma_1$ . Each parametric line is of the form

$$\mathbf{X} = (1 - t_1)\mathbf{X}_i + t_1\mathbf{X}_f \quad (6)$$

where, again,  $\mathbf{X} = [x, y]^T \in \mathbb{R}^2$ ,  $t_1 \in [0, 1)$  represents the interval on which the line is valid,  $\mathbf{X}_i$  represents a point on  $\gamma_0$ , and  $\mathbf{X}_f$  represents a point along the normal projected from  $\gamma_0$ . To ensure that each parametric line is long enough to intersect  $\gamma_1$ ,  $\mathbf{X}_f$  is chosen such that

$$\mathbf{X}_f = \mathbf{X}_i + r\mathbf{N} \quad (7)$$

where

$$r = \max_m \|\mathbf{v}_m - \mathbf{X}_c\| + \frac{1}{2} \left( \max_n \|\mathbf{u}_n - \mathbf{X}_c\| - \min_n \|\mathbf{u}_n - \mathbf{X}_c\| \right) \quad (8)$$

$\mathbf{N}$  is the two-dimensional representation of  $N$  with the  $z$ -component removed, and  $\mathbf{X}_c$  is the centroid of the region enclosed by  $\gamma_0$ .

By a suitable choice of  $r$  we have guaranteed that each parametric line will intersect  $\gamma_1$ . The point of intersection is determined by first equating the parametric line and the spline representing  $\gamma_1$  and then solving for the parametric variables. If we separate the point of intersection into its scalar components (where a subscript of 1 indicates the  $x$ -component and a subscript of 2 indicates the  $y$ -component), we have two equations in two independent variables

$$(X_{f1} - X_{i1})t_1 + X_{i1} = a_1^1t_0^3 + b_1^1t_0^2 + c_1^1t_0 + d_1^1 \quad (9)$$

$$(X_{f2} - X_{i2})t_1 + X_{i2} = a_2^1t_0^3 + b_2^1t_0^2 + c_2^1t_0 + d_2^1 \quad (10)$$

We solve for  $t_1$  in Eq. (9)

$$t_1 = \frac{a_1^1t_0^3 + b_1^1t_0^2 + c_1^1t_0 + d_1^1 - X_{i1}}{X_{f1} - X_{i1}} \quad (11)$$

and substitute  $t_1$  into Eq. (10) which results in the following cubic equation:

$$0 = (a_2^1 - ma_1^1)t_0^3 + (b_2^1 - mb_1^1)t_0^2 + (c_2^1 - mc_1^1)t_0 + (d_2^1 - md_1^1) + (mX_{i1} - X_{i2}) \quad (12)$$

where  $m = (X_{f2} - X_{i2}) / (X_{f1} - X_{i1})$ . The roots of Eq. (12) correspond to the intersection of a spline with the parametric line. In practice, there are  $m - 1$  splines and for a particular normal there are only two roots such that  $t_0 \in [0, 1)$ . If  $t_1$  is further restricted such that  $t_1 \in [0, 1)$ , then there is only one valid root and the intersection point,  $\mathbf{X}$ , can be obtained by substituting  $t_0$  into Eq. (3) or  $t_1$  into Eq. (6). Finally, the Euclidean distance between the point on the initial curve and the intersecting point on the desired curve is calculated.

This process is continued iteratively for each point in  $\mathbf{U}$  and a single VOC is defined which is a bijective mapping of points on the initial curve to the desired curve. Individual layers are generated by appropriate motion along normal vectors that originate on

$\gamma_0$  and terminate on  $\gamma_1$ . For a given point on the initial parametrized curve  $\mathbf{x}_0(t_{x_0})$  and a desired number of layers  $n_d$  each point on a subsequent layer  $\mathbf{x}_i(t_{x_i})$  is defined as

$$\mathbf{x}_i(t_{x_i}) = \mathbf{x}_0(t_{x_0}) + i \frac{\|\mathbf{X}(\mathbf{x}_0(t_{x_0})) - \mathbf{x}_0(t_{x_0})\|}{n_d} \mathbf{n}(t_{x_0}) \quad (13)$$

where  $i = \{1, 2, \dots, n_d\}$  and  $\mathbf{X}(\mathbf{x}_0(t_{x_0}))$  is the point of intersection between the normal line emanating from  $\mathbf{x}_0(t_{x_0})$  and the desired curve. A layer is then defined as the set of all points for a particular  $i$  and, as desired, when  $i = n_d$  we recover the desired curve.

Interestingly, when defined in this manner, each layer is a VOC of the initial curve and the desired curve, but not a VOC of any of the intermediate layers. An exception occurs when the initial and desired curves form an annular region.

**3.2 Three-Dimensional Formulation.** The mathematical formulation for the 3D case is very similar; however, there are three important differences. First, the set of points  $\mathbf{U}$  and  $\mathbf{V}$  must lie on a regular 3D grid. Second, the initial surface must be defined as a piecewise parametric bicubic patch and the desired surface must have an implicit representation, and third, normal vectors must be extended to the 3D case.

For this method, each parametric bicubic patch is described as the tensor product between two different parametric cubic splines,  $\mathbf{R}_1$  and  $\mathbf{R}_2$ . If  $\mathbf{R}_1$  and  $\mathbf{R}_2$  are defined as

$$\mathbf{R}_1(u) = \mathbf{m}_1 u^3 + \mathbf{n}_1 u^2 + \mathbf{l}_1 u + \mathbf{o}_1 \quad (14)$$

and

$$\mathbf{R}_2(v) = \mathbf{m}_2 v^3 + \mathbf{n}_2 v^2 + \mathbf{l}_2 v + \mathbf{o}_2 \quad (15)$$

the bicubic patch is given as

$$\mathbf{X}(u, v) = \mathbf{R}_1(u)\mathbf{R}_2(v) = \sum_{i=0}^3 \sum_{j=0}^3 u^i v^j e_{ij} \quad (16)$$

where now  $\mathbf{X} = [x, y, z]^T \in \mathbb{R}^3$ ,  $e_{ij}$  is the appropriate value for the multiplied spline coefficients from  $\mathbf{R}_1$  and  $\mathbf{R}_2$ , and  $u, v \in [0, 1]$  represent the interval on which the bicubic patch is valid.

Tangent vectors to the parametric surface are calculated by taking the partial derivatives of the bicubic patches

$$\mathbf{T}_1 = \frac{\partial \mathbf{X}}{\partial u} = \left[ \frac{\partial x}{\partial u}, \frac{\partial y}{\partial u}, \frac{\partial z}{\partial u} \right]^T \quad (17)$$

and

$$\mathbf{T}_2 = \frac{\partial \mathbf{X}}{\partial v} = \left[ \frac{\partial x}{\partial v}, \frac{\partial y}{\partial v}, \frac{\partial z}{\partial v} \right]^T \quad (18)$$

Normal vectors are derived by taking the cross product of the tangent vectors in the order that preserves a right-handed frame, i.e.,  $\mathbf{N} = \mathbf{T}_1 \times \mathbf{T}_2$ .

The intersection of the normal vector from the initial surface with the desired surface can be calculated by substituting the coordinates of the parametric line into the implicit equation and then solving the resulting polynomial for the parameter of interest.

## 4 Layer Generation Using Solutions to Laplace's Equation

In this section, we present a method to create layers for nonconvex objects in both two and three dimensions. For this method, layers are defined as modified solutions to Laplace's equation, existing between initial and desired equipotential curves or surfaces, as opposed to VOCs. Although solutions to Laplace's

equation have many practical applications in physical systems such as electrostatics, fluid flow, and magnetostatics and even in control of robotic systems [22–25], to our knowledge, they have not been applied to problems relating to AM processes.

**4.1 Desirable Properties of Solutions to Laplace's Equation.** Laplace's equation is a second-order partial differential equation (PDE) of the form

$$\nabla^2 \phi = \Delta \phi = 0 \quad (19)$$

Any function,  $\phi$ , that is at least twice continuously differentiable and satisfies Laplace's equation is called a harmonic function. Harmonic functions have several desirable properties, but two are of particular interest.

The first property is a corollary of the maximum principle, which states that if a function  $\psi$  is harmonic in a domain  $D$  and continuous in the closure of  $D$ , then both the maximum and minimum values of the function in the closure of  $D$  are attained on the boundary [26]. Furthermore, one can show that a harmonic function, or solution to Laplace's equation, is completely determined by its boundary values. A direct consequence of this fact is that we require only two inputs (i.e., the initial and desired curves or surfaces) to completely define and solve the problem of generating layers. Moreover, since the maximum and minimum values of a harmonic function must be attained on the boundary and we can arbitrarily assign the boundary of the initial and desired objects to have uniform, but different, potentials, we can completely constrain solutions between the two boundaries. In addition, note that we can effectively bound  $\psi$  from above and below by choosing appropriate values for the boundaries of the initial and desired objects. If we further assume that  $\psi$  is continuous throughout the domain, then there exists a continuum of closed equipotential boundaries between the boundaries of the initial and desired objects.

The second property defines the gradient at any point of an equipotential boundary as orthogonal to the boundary. Physically, the gradient of the scalar potential function results in a potential field, existing solely in the domain  $D$ , which is unique at every point. Given a point on the boundary of the initial object and the potential field, we can then construct potential field lines that extend to the boundary of the desired object by integrating. More importantly, these potential lines, originating from different points, do not intersect in the domain.

*Proof.* Assume that two arbitrary potential lines originating from two different points on the boundary of the initial object intersect in the domain at some equipotential boundary. From our previous statement, we affirmed that the gradient at a point on an equipotential boundary is always normal to the boundary. Therefore, after these two potential lines intersect at an arbitrary equipotential boundary they will follow the same path until they terminate on the boundary of the desired object. Since our choice of the intersecting equipotential boundary was arbitrary, it must hold for all equipotential boundaries including the boundary of the initial object. Thus, the two potential lines are the same and must have originated from the same point on the boundary of the initial object, which is a contradiction.  $\square$

With this last property, we can now construct unique, uniformly partitioned layers between an initial and desired object.

**4.2 Formulation.** On 3D Euclidean space, Laplace's equation is given by

$$\nabla^2 \phi(x, y, z) = \left( \frac{\partial^2}{\partial x^2} + \frac{\partial^2}{\partial y^2} + \frac{\partial^2}{\partial z^2} \right) \phi(x, y, z) = 0 \quad (20)$$

where  $\phi(x, y, z)$  is a scalar harmonic function representing a potential field. To solve this PDE for the potential, we must apply

boundary conditions. Therefore, we treat the initial and desired potential surfaces as boundaries and the interior between the two surfaces as free space. Since potential flows from areas of high potential to areas of low potential and we desire the deposited layers to evolve outward from the initial surface, we set the potential on the initial surface to an arbitrary positive value and the potential on the desired surface to zero. Essentially, we want to treat these surfaces as basic Dirichlet boundary conditions.

After solving Laplace's equation, we obtain a harmonic function describing the potential between the initial and desired surfaces. By taking the gradient of the resulting harmonic function, the potential field between the two surfaces can be determined, and by integrating, we can generate potential field lines. Due to the nature of Laplace's equation, the equipotential surfaces are not uniformly spaced and do not lend themselves well to material deposition. This issue is resolved by reparametrizing the potential lines extending between the initial and desired surface by arc length.

If each potential field line is only known for a discrete set of points (as is mainly true for numerical solutions), then we can form a continuous curve by interpolating with piecewise parametric cubic splines. A specific point along the curve is then represented as

$$\mathbf{X}(s) = \mathbf{a}^2 s^3 + \mathbf{b}^2 s^2 + \mathbf{c}^2 s + \mathbf{d}^2 \quad (21)$$

where  $\mathbf{X} \in \mathbb{R}^2$  for the planar case and  $\mathbf{X} \in \mathbb{R}^3$  for the 3D case,  $s$  is arc length at that specific point, and  $\mathbf{a}^2$ ,  $\mathbf{b}^2$ ,  $\mathbf{c}^2$ , and  $\mathbf{d}^2 \in \mathbb{R}^3$  are parameters that uniquely define each potential field line.

The spacing between each layer can be calculated by dividing the total arc length of each potential field line by the desired number of deposited layers,  $n_d$ . Each layer  $\mathbf{L}_j$  is then defined as the set points

$$\mathbf{L}_j = \left\{ \mathbf{X}_k \left( \frac{js_k}{n_d} \right) \right\} \quad (22)$$

where  $j = \{0, 1, \dots, n_d\}$ ,  $k = \{1, 2, \dots, n_f\}$ ,  $n_f$  is the number of potential field lines,  $s_k$  is the total arc length of the  $k$ th potential field line, and  $\mathbf{X}_k(js_k/n_d)$  is the  $k$ th point of the set evaluated at fractional portion of the arc length dependent on the current layer. Note that by using the above definition  $\mathbf{L}_0$  is the initial boundary surface,  $\mathbf{L}_{n_d}$  is the desired boundary surface, and each intermediate surface  $\mathbf{L}_j$  will be uniformly partitioned throughout the medium.

## 5 Incorporating Hollow Features in Build Volumes

As stated earlier, one of the possible benefits of a conformal AM process is the ability to create hollow features. The closest analog in a traditional AM process is holes. Depending on the orientation of the hole relative to the deposition or print head, the hole is either filled with a secondary support material or the print head stops depositing material and is lifted at the edge of the hole and then continues printing on the opposite edge. Although this sort of process is certainly possible in our current framework, the resulting layers are no longer considered conformal as there is a break in the deposition process. Therefore, we seek a method that can effectively deposit layers around the desired hollow feature or void.

**5.1 Limitations.** First, we should note that this method is currently limited to hollow features such that the point at the geometric center is considered compatible (per the definition in Assumption 2 of Sec. 3). And second, this method treats hollow features as local deformations to the pre-existing layers. That is, one of the previous methods (either VOC or Laplace's equation) is used to generate evenly partitioned layers for the volume without hollow features and then this method is applied to generate

local deformations that force the layers around the feature. The tradeoff for being able to conformally deposit material around these hollow features is that the layers are no longer equally partitioned in the local area of the deformations.

**5.2 Formulation.** Although we will only present the 2D formulation of this method in this section, the method is easily extended to 3D by applying the appropriate changes outlined in Sec. 3.2 for the VOC method. First, given a set of ordered points  $\mathbf{O}_i = \{\mathbf{o}_{i1}, \mathbf{o}_{i2}, \dots, \mathbf{o}_{in}\}$  that represent the vertices of  $i$  hollow features, we determine the geometric center  $O_{c_i}$  of each feature as

$$O_{c_i} = \frac{1}{n} \sum_{j=1}^n \mathbf{o}_{ij} \quad (23)$$

where  $n$  is the number of points representing each feature. Then, we dilate the hollow feature by shifting the center to the origin (through a rigid body transformation) and scaling each point by a set factor, typically 1.5, and then shifting back to the original geometric center. This dilated feature is used to create a local "area of effect" (AOE), where points within the area are altered and those outside remain unchanged. Next, both the hollow feature and its dilated representation are approximated as closed curves using piecewise parametric cubic splines following the process outlined in the beginning of Sec. 3.1.

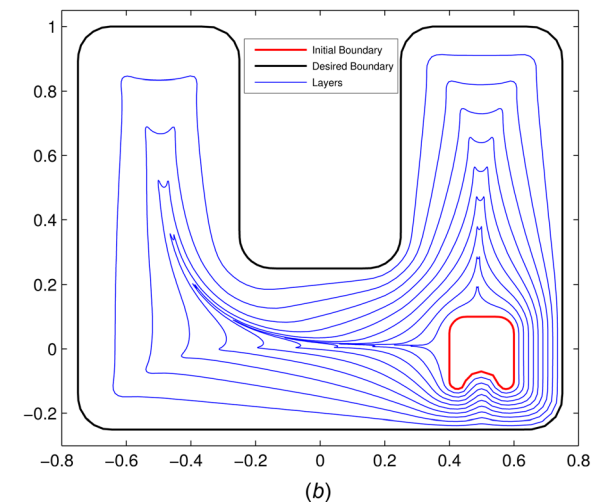
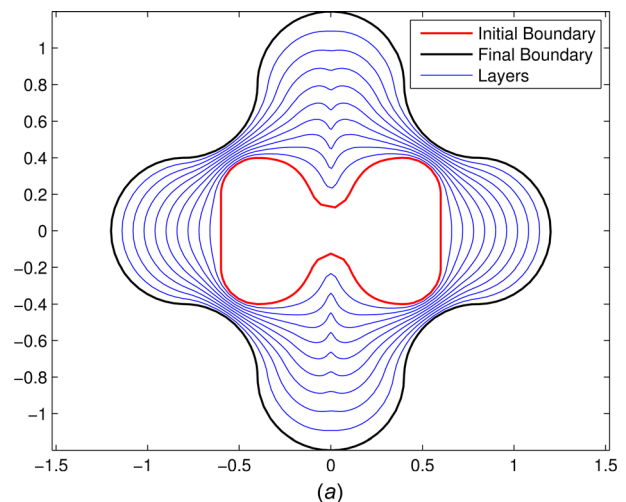


**Fig. 3 Layers generated for arbitrary nonconvex geometries: (a) colocated nonconvex objects and (b) off-center nonconvex objects**

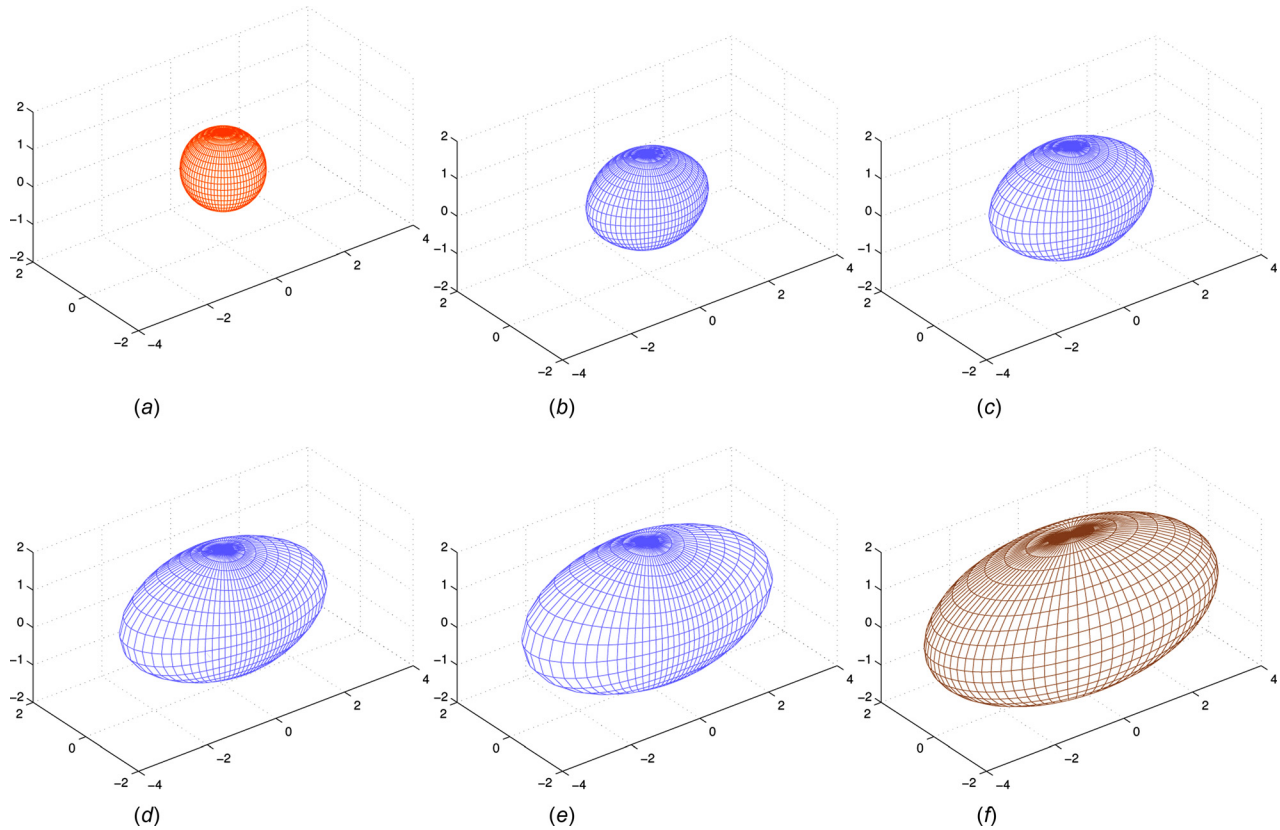


**Fig. 4 Surface evolution of an ellipsoid to a convex surface: (a) initial surface (a sphere), (b) first layer, (c) second layer, (d) third layer, (e) fourth layer, and (f) final layer**

If a point is determined to be within the AOE, the smallest distance from the geometric center of the hollow feature to its boundary and to the boundary of the dilated feature, along a line containing the point of interest, is calculated using the intersection

method outlined in Sec. 3.1. These distances are then used in a parametric line equation to scale the original point to some location between the boundary of the hollow feature and the dilated boundary. The scaling factor is calculated as

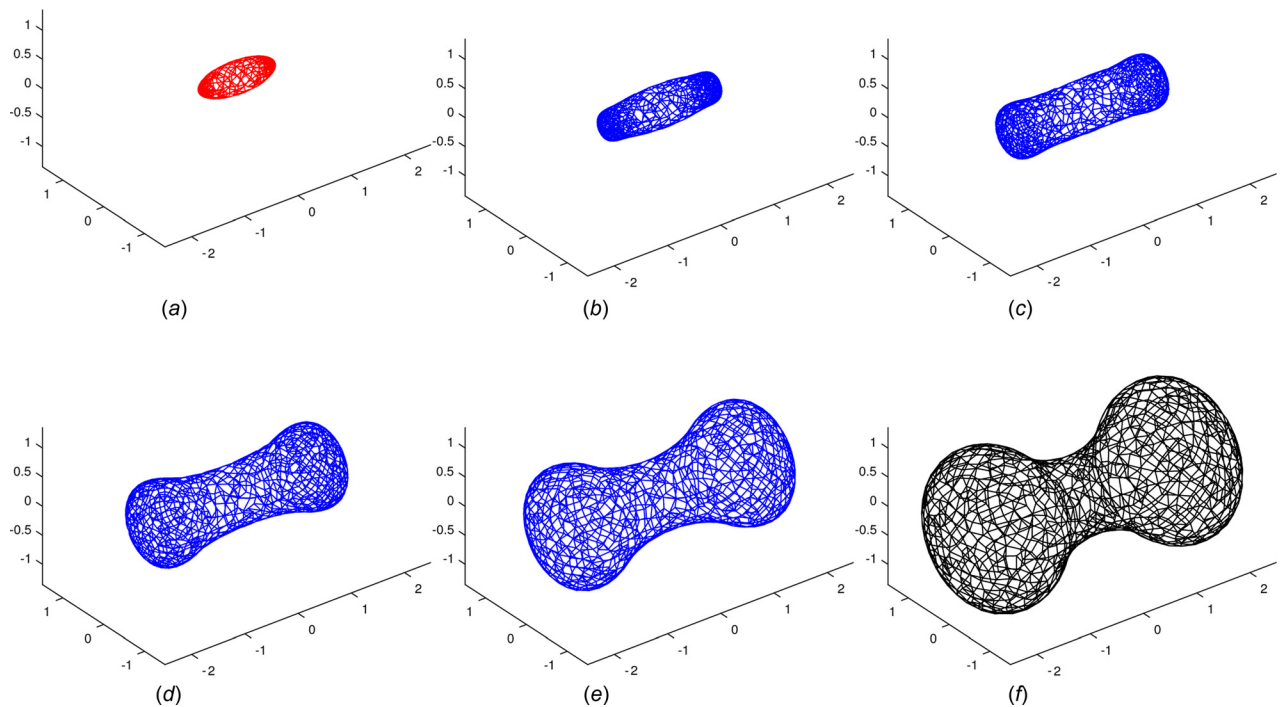


**Fig. 5 Surface evolution of an ellipsoid to a nonconvex surface: (a) initial surface (an ellipsoid), (b) first layer, (c) second layer, (d) third layer, (e) fourth layer, and (f) final layer**

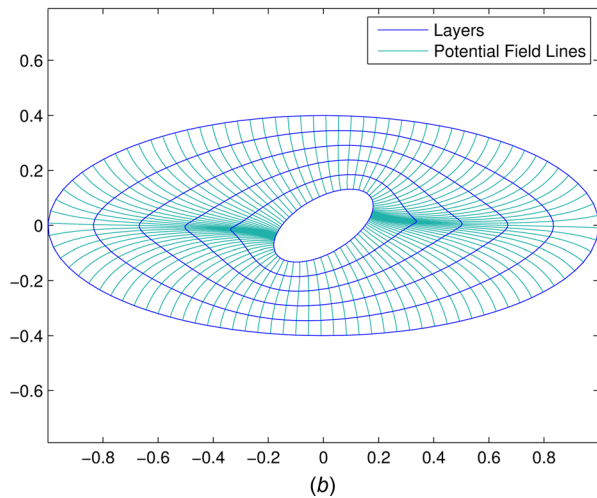
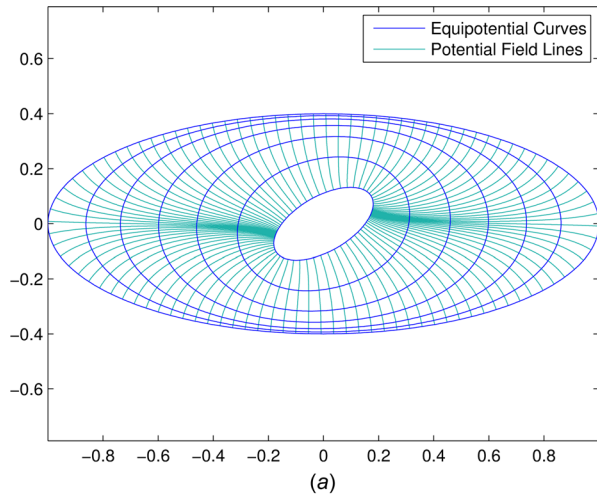


**Fig. 6 Comparison of reparametrized layers for the Laplace's equation method: (a) original equipotential curves and (b) uniformly partitioned layers from reparametrization**

$$s = d_{hf}(1 - t_2) + t_2 d_{df} \quad (24)$$

where  $d_{hf}$  is the distance to the hollow feature,  $d_{df}$  is the distance to the dilated feature, and  $t_2$  is the ratio of the distance from the center of the hollow feature to the point of interest and the distance to the dilated feature. Each point  $p_i$  in the AOE is then transformed by

$$P_i = s \frac{p_i}{d} \quad (25)$$

where  $d$  is the distance from the geometric center of the hollow feature to the point. Intuitively, this transformation moves a point at the geometric center to the boundary of the hollow feature and leaves points on the dilated boundary unchanged. Points in

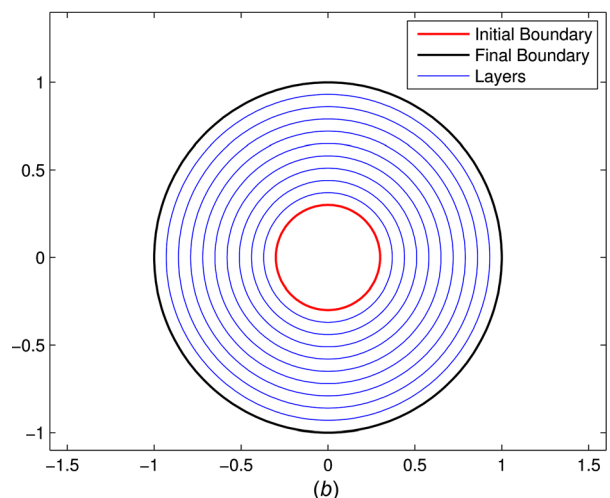
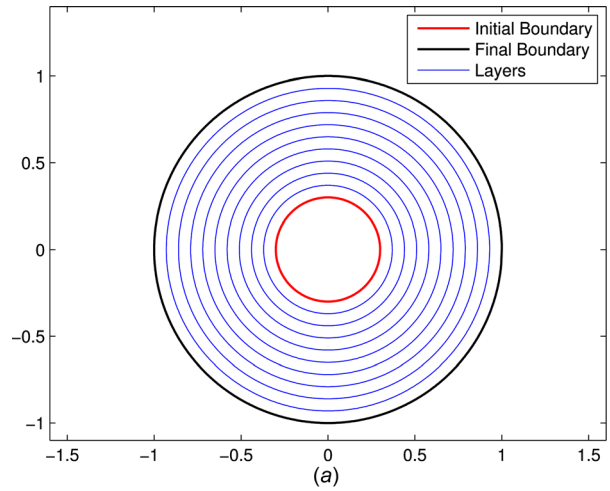


**Fig. 7 Layers generated for an annulus: (a) layers generated by the VOC method and (b) layers generated by the Laplace's equation method**

between these two boundaries are shifted along the line that originates at the geometric center and contains the point of interest.

As currently formulated, the behavior for a point located at the exact geometric center is undefined. For this case, we leverage the fact that these sets of points are in fact individual layers. First, we transform the two adjacent points in the layer. Then, we create a line  $l_1$  between the two points and, finally, we shift the point at the geometric center to the boundary of the hollow feature along the line that bisects  $l_1$ . Another possible concern is when the hollow feature intersects or is tangent to the boundary of the initial object. For this case, any point that is transformed inside of the boundary of the initial object is discarded and no longer part of the layer. A final concern of interest is when one point exists within multiple AOE for different hollow features.

**Table 2 The intersection angle between layers and field lines for ten vertices per layer**

Layer no.	Intersection angle between layers and potential field lines (deg)									
1	44.54	133.99	109.38	97.41	85.51	60.48	40.81	128.63	99.85	91.25
2	44.15	135.68	113.53	97.51	83.99	58.75	42.08	131.78	101.53	91.39
3	52.46	128.26	109.94	95.52	84.76	64.85	50.80	125.42	99.53	91.04
4	67.33	114.03	101.57	92.90	87.00	75.80	65.67	111.65	95.34	90.53
5	90.02	89.61	90.01	90.03	89.96	89.97	90.39	89.98	89.96	90.00

Initially, we experimented by virtually transforming the point for each individual AOE and then shifting the point to the average of the virtual transformations. Due to the different strengths of the virtual transformations, which depend solely on the distance of the point from the boundary of the AOE, this method resulted in layers that oscillated repeatedly in the overlapping AOE. This issue was no less pronounced when weighted averages for each virtually transformed point from each AOE were considered; therefore, an alternate method relying on interpolation was implemented. For each layer, we identified the first and last point that when transformed were located inside of the overlapping AOE. These points and their adjacent points (that remained outside of the AOE) were then used as control points during the interpolation. The untransformed points between the control points were then interpolated over to complete the layer. As a first pass, a linear interpolation method was considered but the resulting discrepancy in the smoothness at the end points was deemed to be too severe. Instead, we implemented a shape-preserving piecewise cubic interpolation method [27] that better preserved the smoothness along the layer. Furthermore, since this method is shape-preserving and it is effectively interpolating over a linear segment in between the control points, the original nonintersecting layers remain nonintersecting after alteration.

## 6 Results

Both methods were simulated to verify their efficacy. The VOC method was solely implemented in MATLAB, while the Laplace's equation method was solved in COMSOL and solutions were manipulated in MATLAB to form uniformly partitioned layers. The remainder of this section is organized as follows: first, we present general examples of layer deposition on arbitrary 2D and 3D objects, next we discuss why results show that the reparametrized solutions of Laplace's equation do not produce orthogonal equipotential boundaries and field lines for intermediate layers, then we compare the results of 2D layer deposition for both methods, and finally we present examples highlighting deposition for two- and three-dimensional objects that include hollow features.

**6.1 Examples of Layer Deposition.** The main advantage of the Laplace's equation method (i.e., deposition between nonconvex objects) is highlighted by depositing ten layers between arbitrary, planar, nonconvex objects in Fig. 3. The deposition of layers onto 3D objects is presented for both methods in Figs. 4 and 5. In Fig. 4, five layers of deposition are applied to a sphere to form a larger ellipsoid using the VOC method. In Fig. 5, five layers of deposition are applied to an ellipsoid to form a larger nonconvex "dumbbell-shaped" surface using the Laplace's equation method.

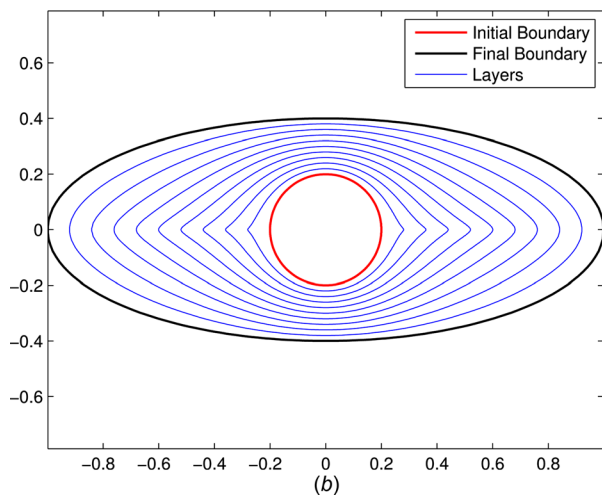
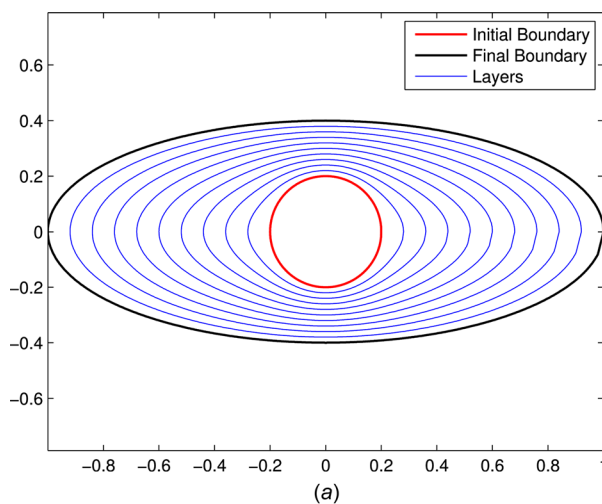


**Fig. 8** The general convexity case: (a) layers generated by the VOC method and (b) layers generated by the Laplace's equation method

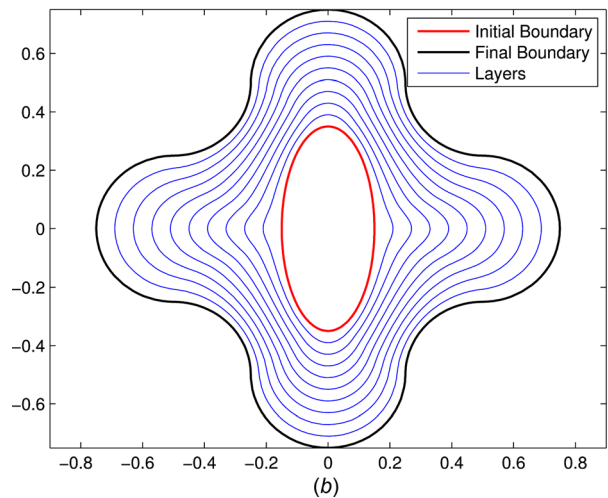
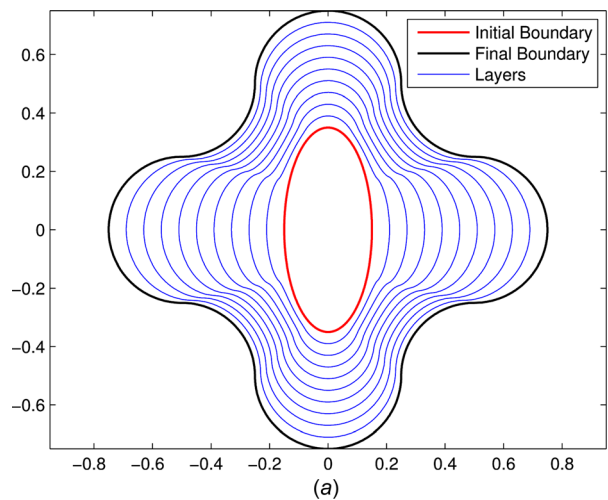


**Fig. 9** The compatible geometric object case: (a) layers generated by the VOC method and (b) layers generated by the Laplace's equation method

In these examples, only five layers were deposited, resulting in large geometric disparities between the layers. Most commercial AM processes can produce layer thicknesses of 0.150 mm or less [28–31], while consumer grade AM processes can typically produce layer thicknesses of 0.2 mm or less [32,33]. Minimum layer thickness varies by AM process and manufacturer; however, thicknesses of less than 0.125 mm are difficult or impossible to achieve. In practice, the number of layers can be chosen to match the layering resolution of the AM process or the layers can be adjusted by the process presented in Ref. [34]. Layers (as defined by this method) need to be greater than or equal to the minimum layer thickness of the AM process.

**6.2 The Nonorthogonality of Reparametrized Laplace’s Equation Solutions.** As discussed previously, potential field lines from Laplace’s equation are orthogonal to each equipotential boundary. However, this property may have been altered when we reparametrized the solution to generate uniformly partitioned layers and by additional sources of error such as numerical

roundoff. A 2D study was conducted to determine if the potential field lines were still perpendicular to each layer. For this study, the initial and desired curves were selected as ellipses and five layers were generated. Figure 6(a) displays the initial equipotential curves before reparametrization and Fig. 6(b) displays the uniformly partitioned layers after reparametrization. Both figures have the same potential lines (which are not altered) in the background.

Visually, it may appear as if the intersections between the potential field lines and layers are orthogonal; however, a numerical study verified that this was not the case. The angle between the potential field lines and layers were calculated for a subset of the vertices via the dot product. Table 2 displays the intersection angle, in degrees, for ten vertices in each layer.

From these results, it is clear that the newly parametrized layers are, in fact, no longer equipotential curves. Reassuringly, the final layer, which was defined as a boundary condition for Laplace’s equation, retains its orthogonality with the potential field lines.

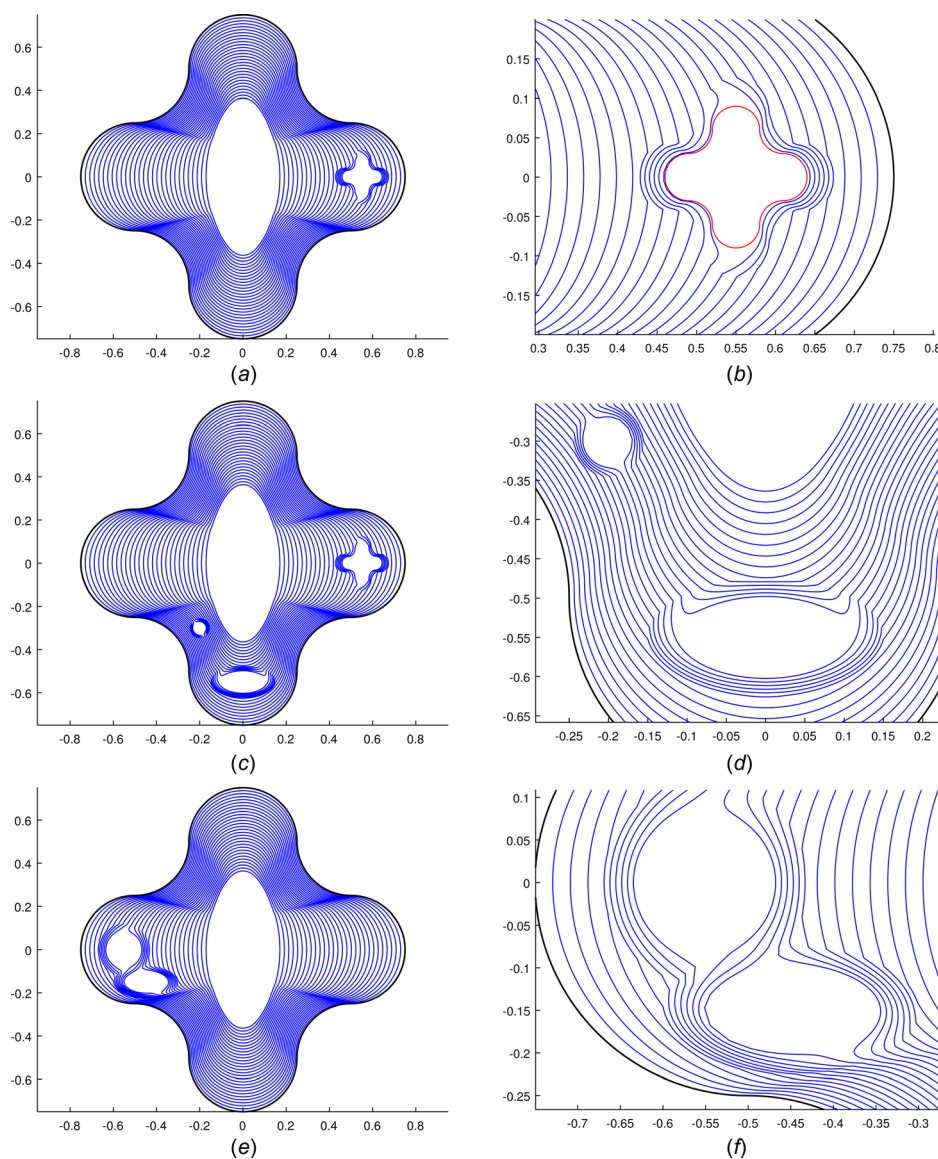


**Fig. 10 Two-dimensional layer generation using the Laplace’s equation method for single and multiple hollow features: (a) layer generation for a single hollow feature, (b) closeup of the layers around a single hollow feature, (c) layer generation for multiple hollow features, (d) closeup of the layers around multiple hollow features, (e) layer generation for overlapping hollow features, and (f) closeup of the layers around overlapping hollow features**

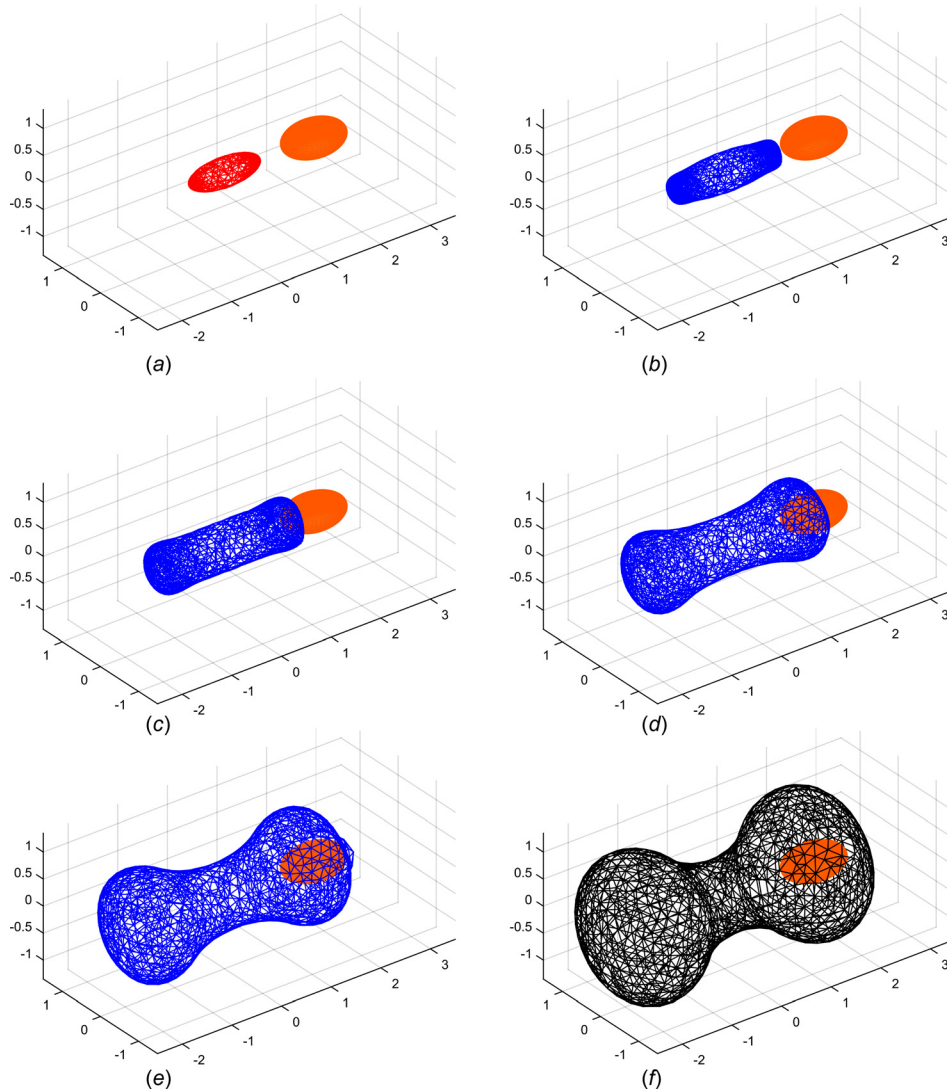


**Fig. 11 Three-dimensional layer generation from an ellipsoid to a nonconvex surface with a single ellipsoidal hollow feature: (a) initial surface (right) with an ellipsoidal hollow feature (left), (b) first layer, (c) second layer, (d) third layer, (e) fourth layer, and (f) final layer**

Although the potential field lines are no longer perpendicular to the intermediate layers, every layer is still unique. The points that define the layers are determined by moving along the unparametrized potential field lines (which were perpendicular to the equipotential boundaries) at different rates corresponding to the distance to the desired curve. As stated earlier, these potential field lines do not intersect one another between the initial and desired curves. Therefore, since each layer evolves outward from the previously defined layer, subsequent layers cannot intersect and are hence unique.

**6.3 Comparison of the Two Methods.** The Laplace's equation method was formulated for nonconvex objects; however, it can also generate layers for convex and compatible objects. Both methods were compared by generating ten layers for planar convex and compatible objects. For the convex case, two geometric objects were tested. First, layers for an annulus were plotted in Fig. 7 and then layers for an ellipse with a circular cutout were generated in Fig. 8. The results clearly display that both methods produce the same results for the annulus, but not for the ellipse.

Returning to an earlier discussion, solutions to Laplace's equation require that equipotential boundaries intersect the potential field perpendicularly. Since the initial curve and desired curve are still considered equipotential curves, the field lines must intersect both curves perpendicularly. In the case of the annulus, normal lines from the initial curve are also normal lines of the desired curve. Therefore, the solutions to both methods are equivalent. The results from the second case confirm this notion, especially along the semimajor axis of the ellipse. Each layer generated by the VOC method is a minimum of  $C^1$  continuous, while only some of the layers from the Laplace's equation method are  $C^1$  continuous. Interestingly, if the layers from both methods are superimposed over one another, the layers exactly overlap on the semimajor and semiminor axes. As before, these locations are where the normal lines from both curves are the same.

For the compatible object case, an ellipse was selected as the initial curve and an adaptation of a "plus" sign was chosen as the desired curve. The layers for each method are presented in Fig. 9. As expected, the layers generated for this compatible geometric object are not identical. Since the VOC method is limited to convex initial curves, there will be no instance where a compatible

desired curve will share all its normal lines with the initial curve. Therefore, there is no compatible geometric object (that is not convex) where both methods will produce the same results.

Although these comparisons were completed for two-dimensional objects, the same results will apply for 3D objects due to the underlying properties of the algorithms.

**6.4 Volumes With Hollow Features.** One of the possible benefits of conformal AM is the ability to create hollow features without the need for sacrificial support material. To demonstrate this capability, we developed a method to generate layers for objects with multiple hollow features given that the point at the geometric center of each hollow feature is compatible (per the definition given in Assumption 2 of Sec. 3). For the time-being, hollow features that do not satisfy these convexity conditions can be still be handled, but a nonconformal process similar to what is currently being used in traditional AM must be employed. Since our method is the same for both the VOC method and the Laplace's equation method, the 2D examples we provide will only be applied to the VOC method, while the 3D example will be applied to the Laplace's equation method. It should be noted that the results for each method will be different, unless the initial layers generated for objects without hollow features are the same. Figure 10 provides three, 2D examples of layer generation using the VOC method from an initial ellipse to a desired star-shape with a different number of hollow features. From Fig. 10, it is evident that our method is able to conformally generate layers around various different types of hollow features at the cost of locally disrupting the even partitioning and smoothness of the layers.

As previously mentioned, each of these 2D examples generalizes to the 3D case and to the Laplace's equation method. Therefore, to minimize redundancy and to highlight the expanded capabilities of the Laplace's equation method, Fig. 11 displays the generated layers for the same initial and desired surfaces used in Fig. 5 with the addition of a single, hollow ellipsoidal feature. During this layer generation process, the layers still evolve from the initial geometric object (an ellipsoid) to the desired object (a dumbbell), but beginning with the second layer the behavior is markedly different than the earlier example. In Fig. 11(c), the layers initially contract away from the hollow feature. But as the untransformed layers transition past the centroid of the hollow ellipsoid as in Fig. 11(e), the transformed layers envelop the remainder of the hollow feature. Once past the AOE of the hollow feature, as in Fig. 11(f), the layer generation behavior again matches that of the previous example.

## 7 Conclusions and Future Work

In this paper, we presented two methods to generate a cascade of enveloping layers between an initial and a desired geometric object. The first method utilized VOCs and was constrained to convex initial geometric objects and either compatible or convex desired objects. The second method manipulated solutions to Laplace's equation to generate layers and was not limited to objects of specific convexities. Notably, the layers that resulted from reparametrizing the solution by arc length were no longer equipotential boundaries; however, each layer remained unique (i.e., did not intersect one another). Then we introduced a method to deal with multiple hollow features inside of the build volume. Examples in both two and three dimensions were presented for each method, including nonconvex geometric objects for the Laplace's equation method and hollow features for both methods. For the 2D case, layers generated by both methods were explicitly compared and a brief discussion extended these results to the 3D case.

The main limitation of the VOC method is its inability to handle nonconvex initial geometric objects, and the restrictions imposed by the compatibility conditions. Future work will aim to resolve these limitations by adaptively modifying the initial and

desired geometric objects into intermediate convex objects that are suitable for our method either by an iterative VOC method or by some other means. The main limitation of the current method based on Laplace's equation is the use of two different software packages. In the near-term, we will develop software that will be solely implemented in MATLAB to reduce computation time and to increase availability and use. Additionally, we will look into the methods that enable our algorithms to deal with hollow features of any convexity.

## Acknowledgment

This work was supported by Johns Hopkins University Applied Physics Laboratory FY14 Independent Research and Development funds and partially supported by the Office of Naval Research FY15 Grant No. N0001415WX01372. Chirikjian's contribution to this material is based upon work supported by (while serving at) the National Science Foundation as an IPA under the IR/D program. The authors thank Bob Matteson, Ryan Forrest, and Paul Biermann for their useful discussions related to this work.

## References

- [1] Kohlmann, L. B., and Lambeth, J., "Providing Rapid Response Solutions for the Fleet Through 3D Printing," United States Naval Institute Blog, United States Naval Institute, Annapolis, MD.
- [2] Freedberg, S. J., Jr., 2014, "Navy Warship is Taking 3D Printer to Sea; Don't Expect a Revolution," Last accessed Apr. 22, 2014, <http://breakingdefense.com/2014/04/navy-carrier-is-taking-3d-printer-to-sea-dont-expect-a-revolution/>
- [3] Cooper, K., 2015, "3D Printing in Zero-G Technology Demonstration," Last accessed Oct 28, 2015, [http://www.nasa.gov/mission\\_pages/station/research/experiments/1115.html](http://www.nasa.gov/mission_pages/station/research/experiments/1115.html)
- [4] ASTM, 2012, "Standard Terminology for Additive Manufacturing Technologies," ASTM International, West Conshohocken, PA, Standard No. ASTM F2792-12a.
- [5] Compton, B. G., and Lewis, J. A., 2014, "3D Printing: 3D-Printing of Lightweight Cellular Composites," *Adv. Mater.*, **26**(34), p. 6043.
- [6] Liang, M., Yu, X., Shemelya, C., Roberson, D., MacDonald, E., Wicker, R., and Hao, X., 2014, "Electromagnetic Materials of Artificially Controlled Properties for 3D Printing Applications," *IEEE Antennas and Propagation Society International Symposium*, Memphis, TN, July 6–11, pp. 227–228.
- [7] Kolesky, D. B., Truby, R. L., Gladman, A., Busbee, T. A., Homan, K. A., and Lewis, J. A., 2014, "Bioprinting: 3D Bioprinting of Vascularized, Heterogeneous Cell-Laden Tissue Constructs," *Adv. Mater.*, **26**(19), pp. 3124–3130.
- [8] Hofmann, M., 2014, "3D Printing Gets a Boost and Opportunities With Polymer Materials," *ACS Macro Lett.*, **3**(4), pp. 382–386.
- [9] Gibson, I., Rosen, D. W., and Stucker, B., 2010, *Additive Manufacturing Technologies: Rapid Prototyping to Direct Digital Manufacturing*, Springer-Verlag, Berlin.
- [10] Radtke, D., and Zeitner, U. D., 2007, "Laser-Lithography on Non-Planar Surfaces," *Opt. Express*, **15**(3), pp. 1167–1174.
- [11] Xie, Y., Lu, Z., Li, F., Zhao, J., and Weng, Z., 2002, "Lithographic Fabrication of Large Diffractive Optical Elements on a Concave Lens Surface," *Opt. Express*, **10**(20), pp. 1043–1047.
- [12] Adams, J. J., Duoss, E. B., Malkowski, T. F., Motala, M. J., Ahn, B. Y., Nuzzo, R. G., Bernhard, J. T., and Lewis, J. A., 2011, "Conformal Printing of Electrically Small Antennas on Three-Dimensional Surfaces," *Adv. Mater.*, **23**(11), pp. 1335–1340.
- [13] Paulsen, J., Renn, M., Christenson, K., and Plourde, R., 2012, "Printing Conformal Electronics on 3D Structures With Aerosol Jet Technology," *Future of Instrumentation International Workshop (FIIW)*, Gatlinburg, TN, Oct. 8–9, pp. 1–4.
- [14] Vatani, M., Engeberg, E., and Choi, J., 2015, "Conformal Direct-Print Piezoresistive Polymer/Nanocomposites for Compliant Multi-Layer Tactile Sensors," *Addit. Manuf.*, **7**(1), pp. 73–82.
- [15] Diegel, O., Singamneni, S., Huang, B., and Gibson, I., 2011, "Curved Layer Fused Deposition Modeling in Conductive Polymer Additive Manufacturing," *Adv. Mater. Res.*, **199**(1), pp. 1984–1987.
- [16] Singamneni, S., Roychoudhury, A., Diegel, O., and Huang, B., 2012, "Modeling and Evaluation of Curved Layer Fused Deposition," *J. Mater. Process. Technol.*, **212**(1), pp. 27–35.
- [17] Kao, J. H., and Prinz, F. B., 1998, "Optimal Motion Planning for Deposition in Layered Manufacturing," *ASME Paper No. DETC98/CIE-5699*.
- [18] Hoschek, J., 1985, "Offset Curves in the Plane," *Comput. Aided Des.*, **17**(2), pp. 77–82.
- [19] Farouki, R. T., and Neff, C. A., 1990, "Analytic Properties of Plane Offset Curves," *Comput. Aided Geom. Des.*, **7**(1–4), pp. 83–99.
- [20] Farouki, R. T., and Neff, C. A., 1990, "Algebraic Properties of Plane Offset Curves," *Comput. Aided Geom. Des.*, **7**(1–4), pp. 101–127.

- [21] Kim, M. S., Park, E. J., and Lim, S. B., 1993, "Approximation of Variable-Radius Offset Curves and Its Application to Bézier Brush-Stroke Design," *Comput. Aided Des.*, **25**(11), pp. 684–698.
- [22] Connolly, C. I., and Burns, J. B., 1990, "Path Planning Using Laplace's Equation," 1990 *IEEE International Conference on Robots and Automation*, Cincinnati, OH, May 13–18, pp. 2102–2106.
- [23] Kim, J., and Khosla, P. K., 1992, "Real-Time Obstacle Avoidance Using Harmonic Potential Functions," *IEEE Trans. Rob. Autom.*, **8**(3), pp. 338–349.
- [24] Keymeulen, D., and Decuyper, J., 1994, "The Fluid Dynamics Applied to Mobile Robot Motion: The Stream Field Method," 1994 *IEEE International Conference on Robots and Automation*, San Diego, CA, May 8–13, pp. 378–385.
- [25] Guldner, J., Utkin, V. I., and Hideki, H., 1997, "Robot Obstacle Avoidance in n-Dimensional Space Using Planar Harmonic Artificial Potential Fields," *ASME J. Dyn. Syst. Meas. Control*, **119**(2), pp. 160–166.
- [26] Nehari, Z., 1952, *Conformal Mapping*, McGraw-Hill, New York.
- [27] Fritsch, F. N., and Carlson, R. E., 1980, "Monotone Piecewise Cubic Interpolation," *SIAM J. Numer. Anal.*, **17**(2), pp. 238–246.
- [28] Stratasys, "Frequently Asked Questions," <http://www.stratasys.com/3d-printers/technologies/fdm-technology/faqs>
- [29] Stratasys, "PolyJet Technology," <http://www.stratasys.com/3d-printers/technologies/polyjet-technology>
- [30] EOS, "EOS M 280," [http://www.eos.info/systems\\_solutions/metal/systems\\_equipment/eosint\\_m280](http://www.eos.info/systems_solutions/metal/systems_equipment/eosint_m280)
- [31] 3DSsystems, "SLA Production 3D Printers," [http://www.3dsystems.com/sites/www.3dsystems.com/files/sla-1113-usen-web\\_1.pdf](http://www.3dsystems.com/sites/www.3dsystems.com/files/sla-1113-usen-web_1.pdf)
- [32] MakerBot, "MakerBot Replicator Mini," <https://store.makerbot.com/replicator-mini>
- [33] 3DSsystems, "Cube," <http://www.3dsystems.com/shop/cube>
- [34] Nelaturi, S., Kim, W., and Kurtoglu, T., 2015, "Manufacturability Feedback and Model Correction for Additive Manufacturing," *ASME J. Manuf. Sci. Eng.*, **137**(2), p. 021015.